Using ion implantation for figure correction in glass and silicon mirror substrates for X-ray telescopes

Brandon Chalifoux*[a], Claire Burch[b], Ralf K. Heilmann[c], Youwei Yao[c], Heng E. Zuo[d], Mark L. Schattenburg[c]
[a]Dept. of Mechanical Engineering, MIT, Cambridge, MA, USA 02139
[b]Harvard University, Cambridge, MA, USA 02139
[c]Space Nanotechnology Lab, MIT Kavli Institute, Cambridge, MA, USA 02139
[d]Dept. of Aeronautics and Astronautics, MIT, Cambridge, MA USA 02139
*bchal@mit.edu; phone: (617) 253-3130; snl.mit.edu

ABSTRACT

Ion implantation is a method of correcting figure errors in thin silicon or glass substrates. For future high-resolution, high-throughput x-ray observatories, such figure correction may be critical for thin mirror substrates. Ion implantation into both glass and silicon results in surface stress, which bends the substrate. We demonstrate that this stress may be used to improve the surface figure of flat glass wafers. We then describe three effects of ion implantation in glass and silicon. The first effect is the stress resulting from the implanted ions, and the implications for figure correction with each material. Second, each material studied also shows some relaxation after the ion beam is removed; we report on the magnitude of this relaxation and its implications. Finally, the surface stress may affect the strength of implanted materials. We report on ring-on-ring strength tests conducted on implanted glass samples.

Keywords: X-ray telescope mirrors, figure correction, ion implantation, glass, silicon

1. INTRODUCTION

The Lynx X-ray telescope mission concept[1] calls for a sub-arcsecond half-power diameter (HPD) angular resolution with large effective area that requires thin mirrors, which have low stiffness. Making sufficiently accurate thin mirrors and maintaining their accuracy through coating, mounting, alignment, and bonding is a challenge that must be solved to make Lynx a realizable mission. At one or more points in the mirror fabrication and integration process, it may be necessary to apply figure corrections to compensate for other errors. One example would be during fabrication of the mirror substrates: if a mirror substrate can be formed (e.g., via glass slumping[2,3,4] or silicon polishing[5]) close to the desired shape, figure correction may improve the mirror figure to achieve the accuracy requirements. Another example would be to apply figure correction via stress-based methods to compensate for stress in the reflective film. Aside from ion implantation, other stress-based methods (e.g., magneto-strictive films[6], or piezoelectric films[3]) or direct methods (e.g., differential deposition[7], ion beam figuring[8]) could also be used to make figure corrections.

In the current work, we use ion implantation to make figure corrections in Schott D-263 glass wafers. In Section 2, we demonstrate that using the process we developed, we can improve the figure of the wafers by 3-5x. However, we also find that, in this material, the post-implant mirror figure changes over the course of days or weeks. In light of this, we explore the possibility of making figure corrections in Corning Eagle XG glass, fused silica, and silicon.

Previously, we have discussed the benefits of the ability to apply non-equibiaxial stress to a surface[9]. For flat wafers, some shapes are simply not correctable with equibiaxial stress. Since Schott D-263 glass exhibits highly non-equibiaxial stress resulting from ions implanted at a non-zero angle of incidence, we could theoretically correct almost any figure error in this material. Eagle XG also exhibits significant non-equibiaxial stress, but fused silica and silicon do not. For these

Optics for EUV, X-Ray, and Gamma-Ray Astronomy VIII, edited by Stephen L. O'Dell, Giovanni Pareschi, Proc. of SPIE Vol. 10399, 103991D · © 2017 SPIE · CCC code: 0277-786X/17/$18 · doi: 10.1117/12.2275324

materials, ion implantation could potentially be used to compensate for stress in a reflective film applied to the mirror, since the film stress should also be nearly equibiaxial. The stress-dose relationship and temporal stability for these materials is shown in Section 3.

Eagle XG glass shows potential as a mirror substrate material that can also be figure-corrected using ion implantation. The stress in the implanted layer, for low ion doses, is tensile. This raises a concern that the strength of the material may be compromised. In Section 4, we show results of strength testing of Eagle XG glass using ring-on-ring bending tests. The strength of the glass does appear to depend on the implanted stress, but the breaking strength of the glass is not significantly compromised.

2. CORRECTION OF SCHOTT D-263 WAFERS

In this section, we present results from correction experiments on glass wafers. Our air bearing slumping effort and initial stress measurements were focused on using flat Schott D-263 glass wafers, so we used this material for these early attempts at figure correction. Using the figure correction process we developed, we were able to achieve a ~3-5x improvement in RMS surface height and RMS slope error. In total, we made corrections on only two wafers before deciding that implanted D-263 glass, unlike other materials we will discuss in Sections 3 and 4, is not stable enough to be practical for a high-resolution x-ray telescope.

The two wafers that we corrected are labeled G2015071503 and G2016070601. Both wafers were slumped at 550 °C with a 0.5 hr dwell time on an air bearing mandrel. The purpose of the slumping is two-fold: first, the initial glass shape (~70 μm P-V) is too warped to be corrected with ion implantation; second, we found a significant difference in the stress-dose relationship for D-263 glass between slumped and un-slumped glass, probably due to internal stress in the un-annealed glass. Sample G2015071503 was coated with 20 nm Cr to ensure a conduction path for ion charges. Sample G2016070601 was spin-coated with PEDOT:PSS, a conductive polymer that may be washed off after use. Both front and back sides of these samples were implanted, which was necessary based on the initial shape of the glass wafer.

2.1 Correction process for Schott D-263 glass

The correction process for Schott D-263 glass is illustrated in Figure 1. For all materials, this process will be similar. This process was described previously[10] and summarized here.

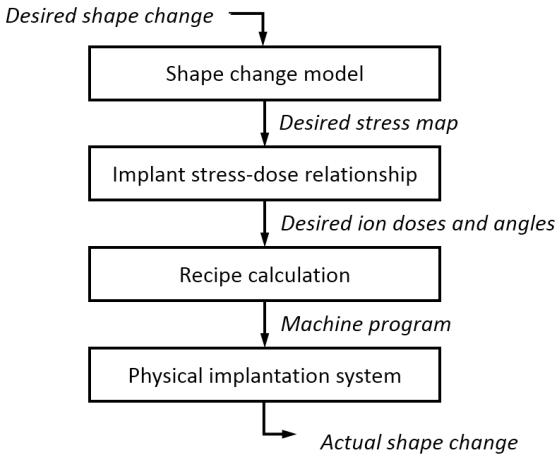

Figure 1. Block diagram of the ion implantation figure correction process.

1. **Stress field calculation.** The first step is to calculate a stress map that is attainable and that causes a desired deformation. This stress map is not unique, and may be calculated numerically using discrete influence functions[11] or continuous functions[9].
2. **Ion dose and ion beam angle calculation.** Next, using measured stress-dose relations at various ion beam angles of incidence, such as that shown in Figure 2, we calculate all possible sets of ion doses and ion beam angles that achieve the desired stress state established in step 1.
3. **Recipe calculation.** Next, a sequence of ion beam positions on the substrate, ion beam angles, and ion doses must be found that can be implemented on the physical implantation system[9]. This system cannot move the substrate infinitely fast, so we must keep the changes in angles between subsequent ion beam positions small to minimize ion dose error. In addition, we must de-convolve the measured ion beam profile from the desired dose and angle map, to get the number of ions to be implanted at each location. We then write a machine-language program (AeroBasic) to be loaded onto the motion controllers.
4. **Physical implantation.** The recipe program is loaded onto the ion implantation machine's motion controllers. The ion accelerator is set up to provide a continuous beam of high-energy ions (in this case, 6 MeV O^{3+}), and the machine program is run, which moves the wafer to a desired set of angles while simultaneously steering the ion beam using electrostatic steering plates. The ion beam and sample are held at each position until the desired number of ions are implanted at that location.

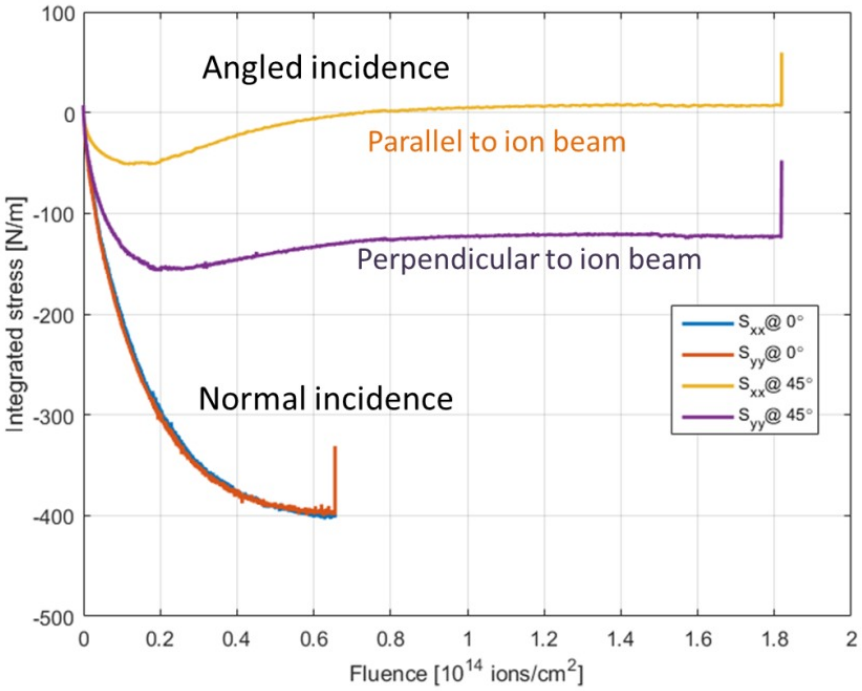

Figure 2. Stress-dose relationship for Schott D-263 glass implanted with 6 MeV O^{3+} ions at a 45° angle of incidence and a 0° angle of incidence. The integrated stress in two directions on the glass surface is calculated from in-situ 2-D curvature measurements. The vertical spikes at the end of each data set are the result of post-implant deformations, which are discussed in Section 3.

2.2 Correction results

Two wafers were measured before and after correction, using a Shack-Hartmann metrology tool[12], which measures surface slopes. The surface slopes are fit to a set of Zernike polynomials up to 4th order to obtain the surface height map. The surface maps of both wafers before and after correction are shown in Figure 3. The corrected wafers were monitored for several days after the correction, and they were found to change. One wafer, G2015071503, was found to be changing

even two weeks later. The RMS height and RMS surface slopes are shown as a function of time in Figures 4 and 5. Even when these values appear relatively constant, the surfaces can still be changing. For both wafers, the ratio of the original RMS height or RMS slope to the corrected RMS height or RMS slope was better than a factor of 2-3 initially, but degraded in both cases.

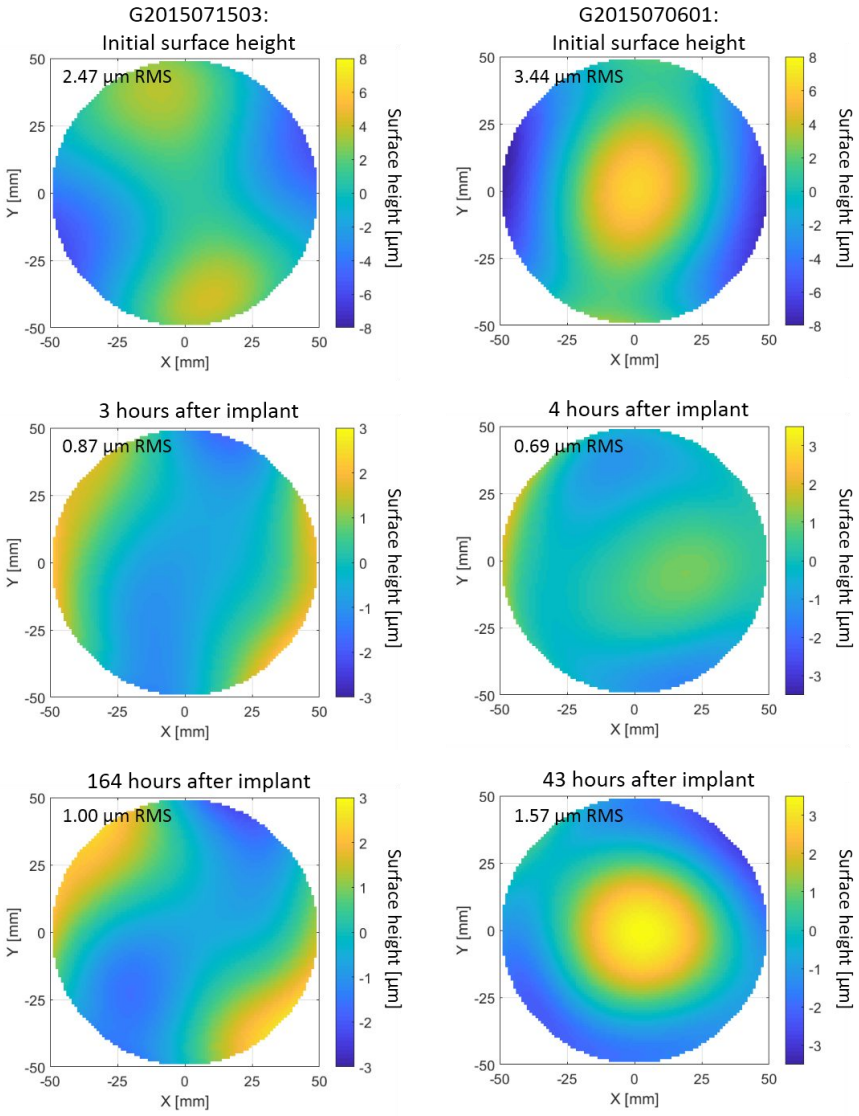

Figure 3. Surface maps of two corrected D-263 wafers, showing continuing change even after a few days. Note that the scale changes between the initial surface maps and the post-implant surface maps.

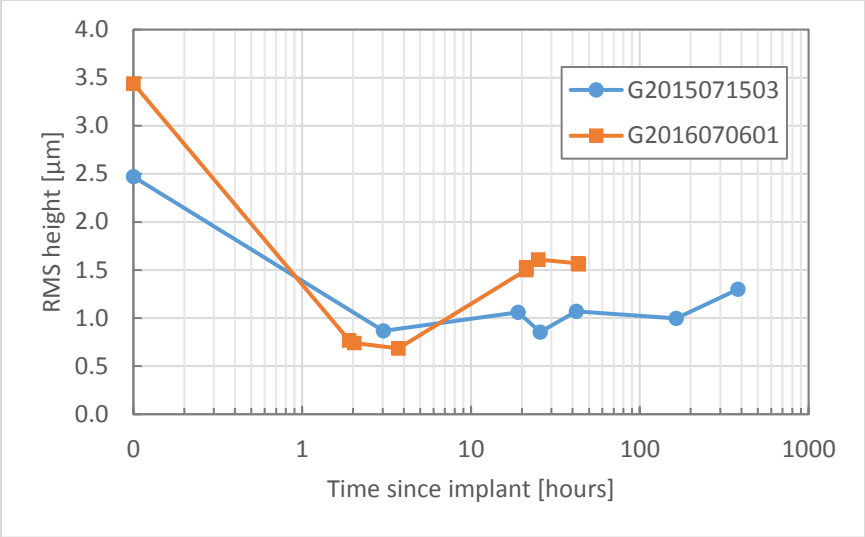

Figure 4. RMS surface height as a function of time since the correction, for both wafers. The first data point is from the pre-implant surface measurement.

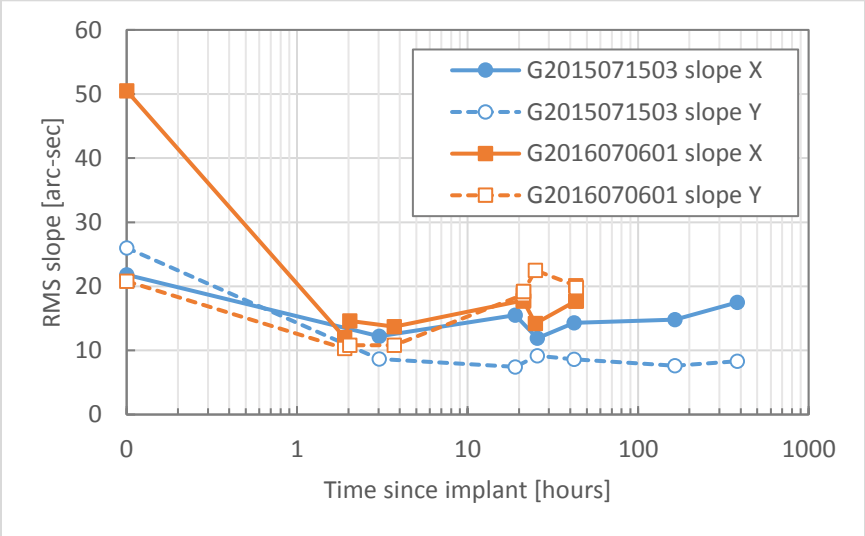

Figure 5. RMS surface slopes as a function of time since the correction, for both wafers. The first data point is from the pre-implant surface measurement.

These corrections demonstrate that the surface figure of air-bearing slumped Schott D-263 glass wafers can be improved by a factor of two or more using ion implantation. Despite this, we chose to move away from using Schott D-263 glass for ion implantation since the glass shape continues to change for a very long time after ion implantation.

Post-implant changes in Schott D-263 glass are difficult to predict, since the time-scales for the changes are very long. In order to adequately predict these changes, we would need to measure many implanted wafers over several weeks (at least). The wafers would need to be implanted to various doses and at various angles of incidence, and the metrology system must be able to measure these changes accurately over this time period. Instead, we chose to explore the use of other glass types, and we show results for these in Section 3.2. We find that both Corning Eagle XG glass and fused silica show significantly lower magnitudes of post-implant changes than Schott D-263 glass.

3. STRESS-DOSE RELATIONSHIP FOR GLASS AND SILICON

Using in-situ curvature measurements, we measured the stress-dose relationship, and the post-implant changes, for Schott D-263 glass, Corning Eagle XG glass, and fused silica implanted with 6 MeV O^{3+} ions. Eagle XG and D-263 glass exhibited significant non-equibiaxial stress when implanted at a 45° angle of incidence, but fused silica did not. As discussed previously[9], this theoretically enables complete correction of Eagle XG and D-263 glass. Both Eagle XG and fused silica showed significantly smaller post-implant changes than Schott D-263 glass.

3.1 Stress in glass: D-263, Eagle XG, and fused silica

We simultaneously implanted ions into square (20 mm x 20 mm x 0.5 mm) glass samples and measured the change in curvature of these samples. The samples were coated with 20 nm Cr on the implanted side to avoid charge build-up and to provide a reflective surface for curvature measurement. The samples were measured using an in-situ curvature measurement device, which is illustrated in Figure 6a. The device is essentially a Shack-Hartmann wavefront sensor. A 25 mm diameter collimated 635 nm laser beam is reflected off of the sample, magnified with a telescope, and sub-apertured by a microlens array. The focal spots from the microlens array (raw image shown in Figure 6b) are tracked during the ion implantation, and the change in focal spot centroid is related to the local change in surface slope of the sample.

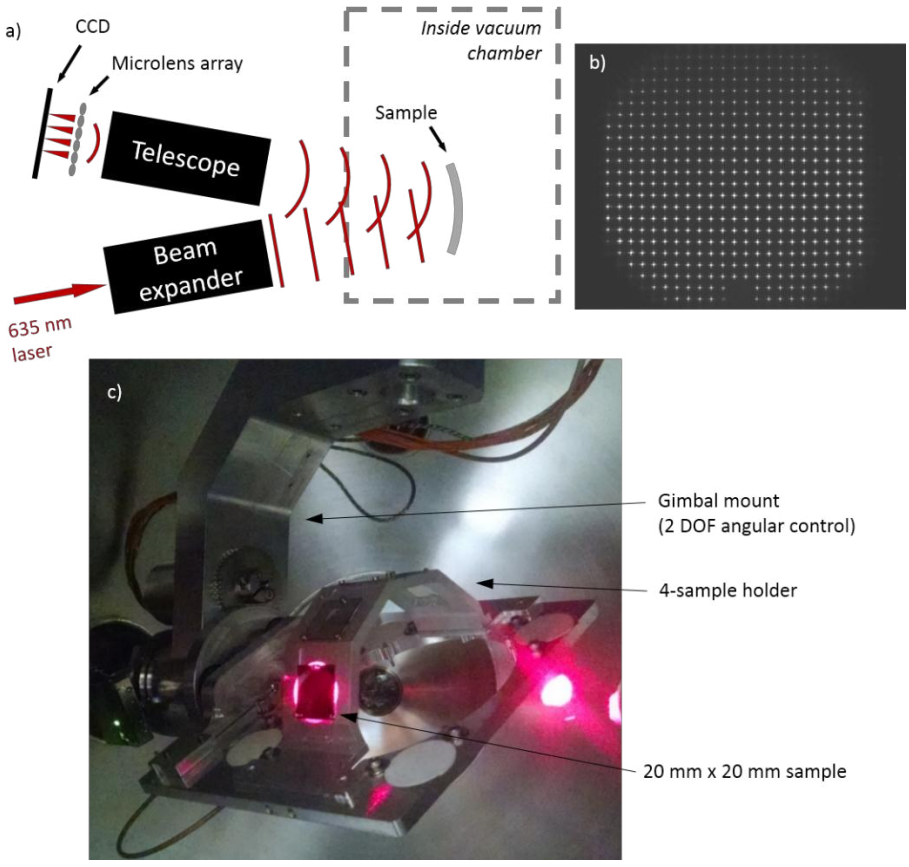

Figure 6. In-situ curvature measurement setup. a) A Shack-Hartmann setup measures sample curvature changes by reflecting a collimated laser beam off of the sample, and measuring the curvature of the reflected sub-apertured wavefront on a camera. b) The raw image consists of a grid of focal spots, which are tracked to determine the local slopes of the sample. c) a sample holder holds four samples (mounted on steel balls and held on by small disc magnets) and allows rapid switching between samples to enable efficient post-implant relaxation measurements.

Using the surface slopes of the sample, three average curvatures may be calculated (alternatively, one may think of this as fitting power and two astigmatism terms to the slopes). The integrated stress in each direction may be calculated using a modified Stoney's equation[13],

$$S_{xx} = \frac{E_s h_s^2}{6(1-\nu_s^2)}\left(\kappa_{xx} + \nu_s \kappa_{yy}\right),$$

$$S_{yy} = \frac{E_s h_s^2}{6(1-\nu_s^2)}\left(\kappa_{yy} + \nu_s \kappa_{xx}\right),$$

$$S_{xy} = \frac{E_s h_s^2}{3(1+\nu_s)}\kappa_{xy}.$$

Here, $S_{xx}, S_{yy}, \kappa_{xx}$ and κ_{yy} are the normal integrated stresses (also called film force, and equivalent to film stress multiplied by film thickness) and curvatures in the x- and y-directions, respectively, and S_{xy} and κ_{xy} are the shear integrated stress and twist curvature, respectively. E_s is the substrate elastic modulus, h_s is the substrate thickness, and ν_s is the substrate Poisson's ratio. While we calculate the twist curvature and shear integrated stress, the measurements are always nearly zero as expected, so we do not include them in any plots in this paper.

The ion beam, typically focused to about 3-5 mm diameter, is scanned over the sample using a sawtooth pattern in both x- and y- directions. The ion flux is measured using a picoammeter, which is the only path to electrical ground for ion charges hitting the sample. The sample is held at +500V during the implantation to ensure that secondary electrons, ejected from the sample due to the high energy ions, are returned to the sample, to ensure accurate ion flux measurement.

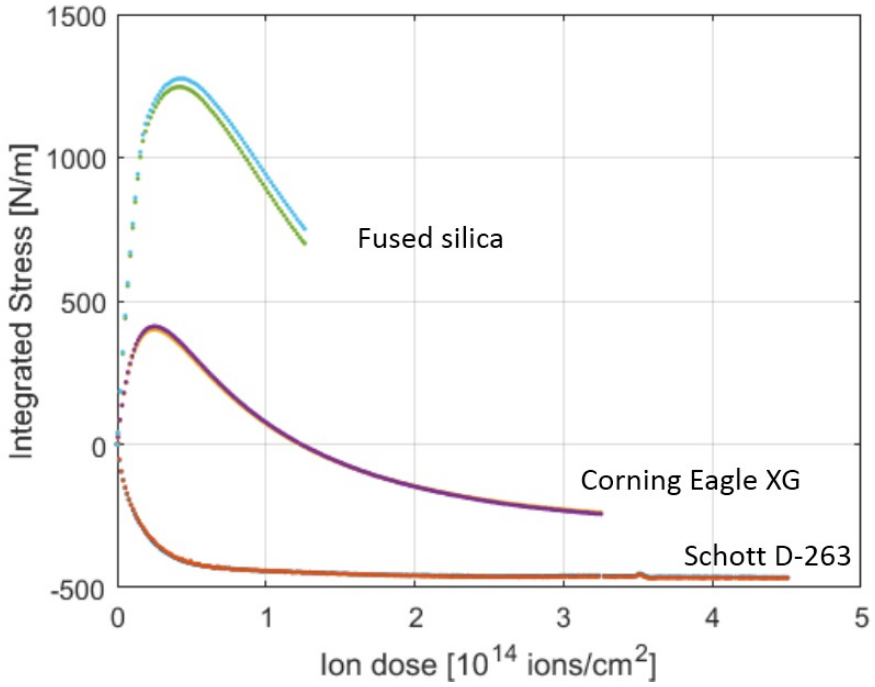

Figure 7. Integrated stress as a function of ion dose in fused silica, Corning Eagle XG, and Schott D-263 glass, showing significant dependence on the glass type. These samples were implanted at a 0° angle of incidence, with 6 MeV O^{3+} ions. The two colors for each material represent the curvature measured in the vertical and horizontal directions (corresponding to the colors in Figure 8).

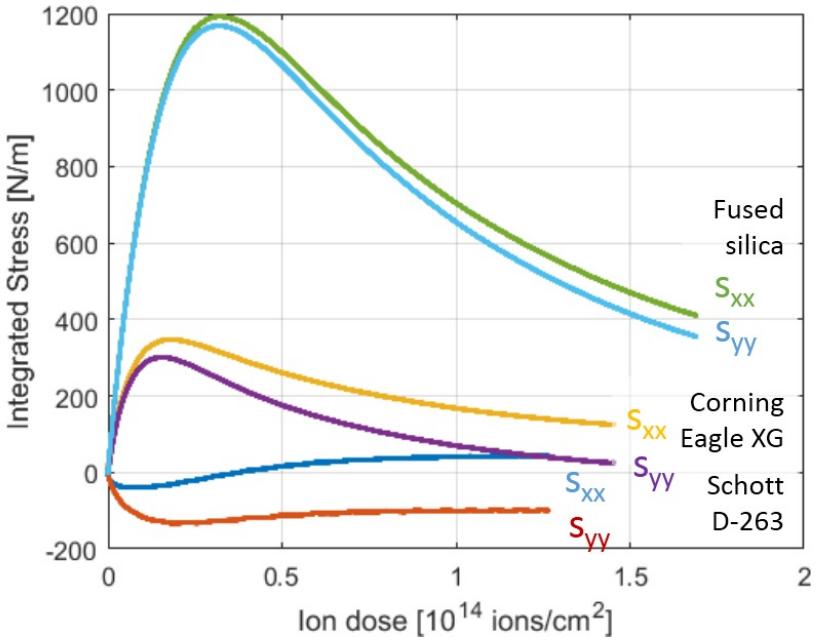

Figure 8. Integrated stress as a function of ion dose in fused silica, Corning Eagle XG, and Schott D-263 glass, showing significant dependence on the glass type. These samples were implanted at a 45° angle of incidence, with 6 MeV O^{3+} ions.

We measured integrated stress as a function of ion dose in three types of glass: Corning Eagle XG, Schott D-263, and fused silica. We measured the stress-dose relationship for a normal-incidence ion beam (0° angle of incidence, 6 MeV O^{3+} ion beam, 70 nA ion current) and an angled ion beam (45° angle of incidence, 6 MeV O^{3+} ion beam, 70 nA ion current). The data are shown in Figures 7 and 8, respectively. Each material shows quite different behavior, demonstrating a strong material dependence.

Schott D-263, implanted with a normal-incidence ion beam, monotonically develops a compressive equibiaxial stress. Corning Eagle XG and fused silica both develop a tensile equibiaxial stress. We did not measure fused silica to a high ion dose (but other researchers[14] have), but Corning Eagle XG at least eventually develops a compressive stress. The compressive stress results from a thermal spike effect, which also causes non-equibiaxial stress with an angled ion beam, as we have discussed previously[9]. The non-equibiaxial stress is the difference in integrated stress between the x- and y-directions. At angled incidence, Schott D-263 develops a large non-equibiaxial integrated stress. Corning Eagle XG develops a smaller non-equibiaxial integrated stress, and fused silica develops the smallest non-equibiaxial stress. All three could be used with ion implantation figure correction. In the next section, we discuss the differences in post-implant stability of each of these materials.

3.2 Comparison of post-implant changes in different glasses

When the ion beam is removed, the curvature of all samples changes. The changes approximately follow an exponential decay. We measured the post-implant changes in curvature of Schott D-263, Eagle XG, and fused silica samples. Figure 9 shows a comparison of post-implant changes in integrated stress for the three samples shown in Figure 8. Each sample was implanted at an angle of incidence of 45° to approximately the same ion dose. It is clear that Schott D-263 glass relaxes significantly more than Eagle XG glass or fused silica, but the post-implant relaxation of Eagle XG is not negligible.

Both Eagle XG and Schott D-263 show non-equibiaxial relaxation for implants at a 45° angle of incidence. In all cases, for all of the glass materials we tested, the relaxation is positive, regardless of whether the stress was positive or negative when the ion beam was removed. This indicates that this relaxation is not the result of viscous relaxation of stress, which would depend on the sign of the initial stress. The relaxation roughly follows an exponential decay initially, but in both Corning Eagle XG and Schott D-263, the relaxation appears to reach a logarithmic asymptote (a straight line on a log scale). We find this is the case for Eagle XG even after four days, but we do not know if this continues indefinitely.

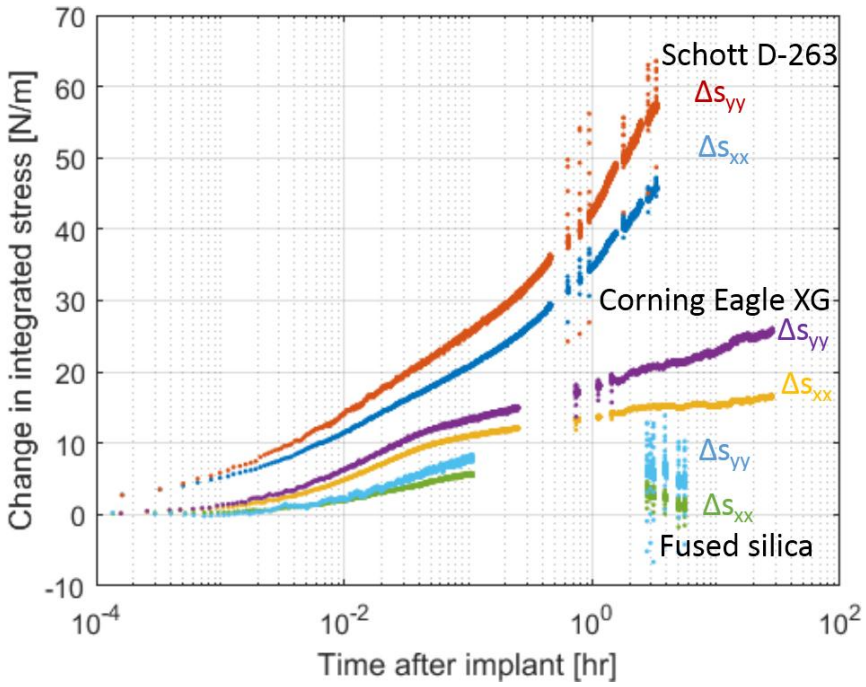

Figure 9. Post-implant stress relaxation in Schott D-263, Corning Eagle XG, and fused silica glass. These are the same samples shown in Figure 8; each sample was implanted at a 45° angle of incidence to approximately 1.5 x 10^{14} ions/cm^2 before the ion beam was removed. The changes in integrated stress are non-equibiaxial, and always positive. These samples were measured intermittently after the first 30 minutes, which results in significant noise, but the relative magnitudes of relaxation are clear.

For Eagle XG, sample curvatures were measured for four days using the following procedure. Once the sample is implanted to the desired dose, the ion beam is blocked or steered off of the sample, and the sample is monitored for about 15 minutes to capture the initial post-implant curvature changes. Then the next three samples are implanted to the desired dose, and 15 minutes of post-implant relaxation is captured for each. Then, for four days, each sample is alternately cycled into the measurement position for several minutes.

Seven samples were implanted with 6 MeV O^{3+} ions at a 45° angle of incidence, to various ion doses, before the ion beam was removed. The measured change in integrated stress, in both directions, is shown in Figure 10. As noted above, the change in integrated stress when the ion beam angle of incidence is 45° is not equibiaxial (i.e., the integrated stress changes in each direction are not the same). Figure 10 shows a clear dependence of the post-implant changes on the implanted dose.

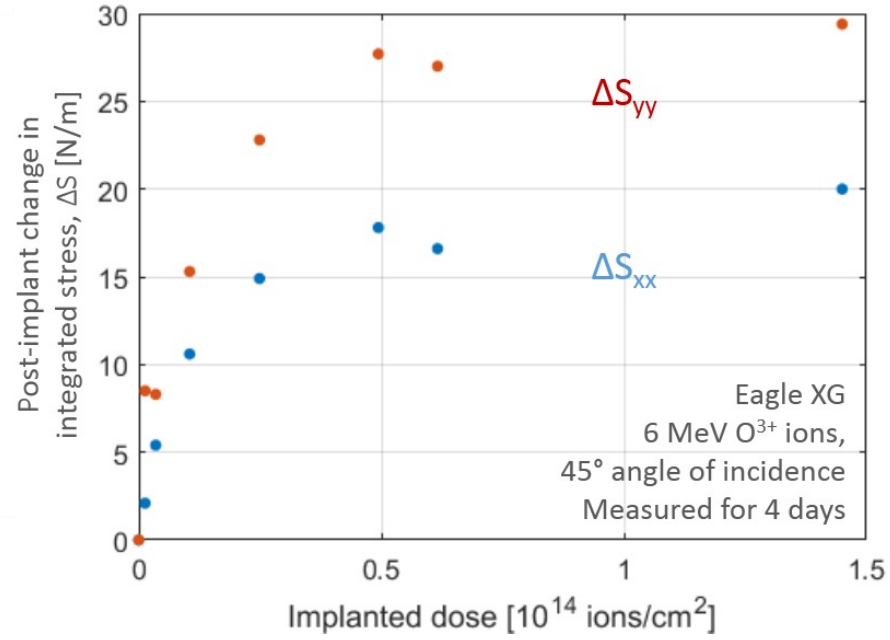

Figure 10. Post-implant changes in integrated stress of Corning Eagle XG glass samples, measured 4 days after implant. The samples were implanted with 6 MeV O^{3+} ions at a 45° angle of incidence, to various doses before the ion beam was removed.

If we were to correct Eagle XG glass mirror substrates, it would be necessary to anticipate these post-implant figure changes when calculating an implant recipe. For correcting D-263 glass wafers, we attempted to compensate for the expected post-implant changes. Howver, we did not measure the post-implant changes over a sufficiently long period of time, and we under-estimated the magnitude of these changes.

3.3 Stress in silicon

Silicon is rapidly becoming an important candidate material for high resolution, thin x-ray telescope mirror substrates[4]. Our early work on ion implantation used silicon substrates[15], and we found that integrated stress could be applied using 150 keV Si ion beams, as other researchers have observed[16]. Our current work is on using our implantation chamber at MIT, which is attached to an ion accelerator that can produce MeV silicon ion beams.

Ion implantation results in an equibiaxial integrated stress in silicon. One application of ion implantation in silicon may be to counter the deformation that results from applying a reflective film such as iridium, since the film stress is probably equibiaxial, or nearly so. Other researchers[17] have investigated applying a nominally equivalent stressed film to both sides of a mirror substrate, and found that the stress does not cancel. This may be a result of non-uniformity in the film stress or film thickness, or dependence on the curvature of the substrate. With ion implantation, we may easily apply a non-uniform integrated stress distribution after the reflective film has been deposited. With a film stress[18] of ~2 GPa (compressive) and a thickness[19] of 15 nm, we would need to apply approximately -30 N/m to the other side to counter the film stress.

For curved mirrors, we would also like to have the mirror oriented normal to the ion beam, a position in which we cannot measure the mirror surface. For in-situ curvature measurements, then, we alternate between implanting and measuring. We implanted 6 MeV Si^{3+} ions at normal-incidence, into a 100 mm diameter 0.3 mm thick silicon <1 0 0> wafer, at 500 nA of beam current. The measurement time was 30 seconds, and the implant time was 300 seconds. The total implant time was less than two hours, and could likely be significantly reduced. Figure 11 shows the stress-dose relationship for this particular wafer, after we averaged the curvature measurements from each measurement period.

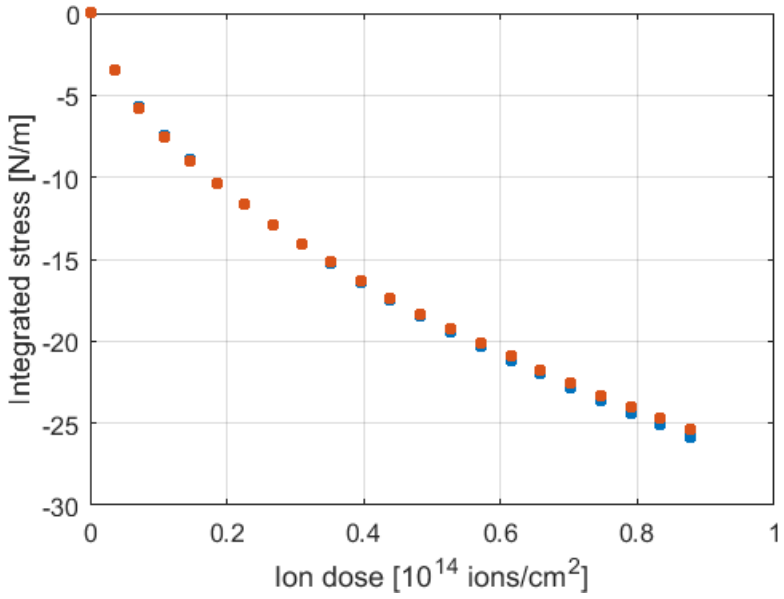

Figure 11. Stress-dose relationship for 6 MeV Si^{3+} ions implanted at normal-incidence into a <1 0 0> silicon wafer.

After the ion beam was removed, we measured the change in integrated stress as with glass. The measurements are shown in Figure 12. Compared with the relaxation data shown in Figure 9, the magnitude of change for silicon is quite small. There is a 24-hour periodicity of drifting in the post-implant stress data, suggesting that better thermal control would improve the stability of this measurement. There is certainly some initial change after the ion beam is removed, but after this, the changes are uncertain due to measurement drift. The observed changes might simply result from thermal effects, but we have not yet explored this. In any case, it is clear that the changes are small, on the order of 1 N/m.

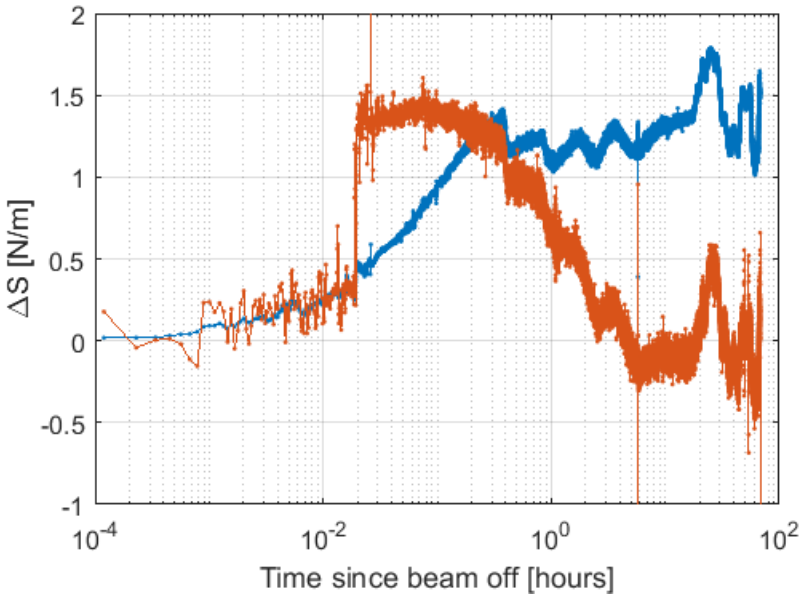

Figure 12. Post-implant changes in integrated stress of a silicon <1 0 0> wafer, measured for 3 days. The wafer was implanted with 6 MeV Si^{3+} ions at a 0° angle of incidence to a dose of 7 x 10^{13} ions/cm² before the ion beam was removed.

4. STRENGTH OF IMPLANTED EAGLE XG GLASS

Corning Eagle XG glass is a promising material for thin x-ray telescope mirror substrates, as well as for correction with ion implantation. This material is currently being used as substrates for active x-ray telescope mirrors[3]. However, one concern is that the large tensile stress applied to the surface via ion implantation could significantly weaken the glass and limit its use for a telescope application. In this section, we present results from strength tests applied to unimplanted and implanted Eagle XG glass samples. We find that there is some weakening, but it is small compared to the spread in the strength data.

4.1 Measurement procedure

We loaded to failure 26 square (20 mm x 20 mm x 0.5 mm) samples of Corning Eagle XG glass. The samples were cut from three 100 mm Corning Eagle XG glass wafers with 20-10 scratch-dig surface quality. The treatments for each wafer are summarized in Table 1. The samples were split into three categories: unannealed and unimplanted, annealed and unimplanted, and annealed and implanted. The implanted samples were implanted with a normal-incidence ion beam (see Figure 7 for the stress-dose relationship at normal-incidence for Corning Eagle XG glass). Each sample was implanted with a different dose, and the integrated stress was measured in-situ.

Table 1. Treatment parameters for the three Corning Eagle XG glass wafers from which samples were cut for strength testing.

	Wafer 1	Wafer 2	Wafer 3	Comments
Thickness [mm]	0.50	0.50	0.50	
Coating	20 nm Cr (e-beam evaporated)	20 nm Cr (e-beam evaporated)	20 nm Cr (e-beam evaporated)	Coating for charge dissipation during implant
Annealing	None	4 hr rise to 740 °C, 8 hr cool to 700 °C	4 hr rise to 740 °C, 8 hr cool to 700 °C	Annealed on Pt-coated silica.
Number of implanted samples	0	1	7	Implanted on mandrel side
Number of strength-tested samples	9	8	9	Tensile face on mandrel side

The sample loading apparatus, which uses a ring-on-ring loading architecture, and setup are shown in Figure 13 and follow guidelines from the ASTM C1499 standard. A load ring (8 mm diameter) applies force to a sample that is resting on a support ring (16 mm diameter). Both rings are machined out of aluminum and have a 0.5 mm radius of curvature. The ring-on-ring test is designed to load a region of a sample to uniform stress, without inducing significant stress at the edge of the sample. This is particularly important for brittle samples like glass, in which edge cracks can propagate at much lower stress than the breaking strength of the glass. Unless stress at the edges is minimized, strength tests can represent the edge-preparation processes more than the actual strength of the glass. For small deformations of the sample, the ASTM C1499 standard results in relatively uniform stress in the region of the sample inside the load ring. As will be discussed later, however, thin glass samples undergo large deformations, which results in non-uniform stress in the center region, which must be accounted for.

The instrumentation consists of a load cell (range: 450 N, resolution: 0.2 N) for force measurement, and three capacitance gauges (range: 2.5 mm, resolution: 5 μm) for displacement measurement. The load cell is held in a milling machine spindle with a motorized vertical axis (speed: 50 μm/sec), and the sample loading apparatus is held in the milling machine vise. As stipulated in ASTM C1499, there is a ball between the load cell and the top plate of the sample loading apparatus, to uniformly distribute the loading on the glass. The top side of the samples (which is the side under compression and therefore unlikely to initiate a fracture) are covered with a thin piece of Teflon tape to minimize the effects of friction, in accordance with ASTM C1499. Likewise, the support ring (larger diameter) is covered with Teflon tape.

The test begins by placing a sample on the support ring, with the implanted (if applicable) side facing down. The sample is aligned by eye to a square template machined into the fixture. The load ring plate is added and aligned to the bottom plate with an alignment fixture. A ball is placed in a conical divot in the center of the load ring plate, and the load cell is lowered slowly until a reading of ~1 N is registered. The data acquisition for force and displacement is started. The load cell is then lowered at a rate of 50 μm/sec until the sample breaks.

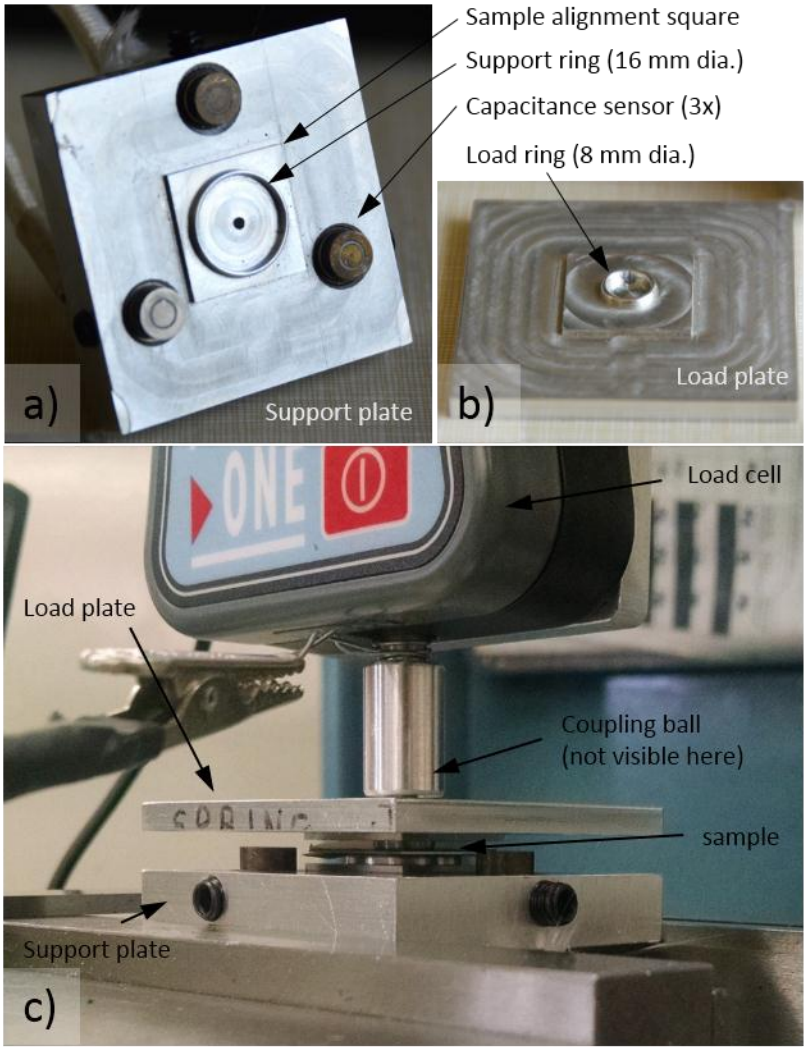

Figure 13. Photographs of glass strength testing setup. a) The support ring plate contains a machined aluminum support ring, an alignment feature, and three capacitance sensors. b) The load ring plate contains a machined aluminum load ring and an alignment feature. c) The assembly consists of a support ring (held in a vise), a thin glass sample, the load plate, a coupling ball, and a load cell.

4.2 Results and discussion

We measure the maximum load, but we are interested in the breaking strength in the glass. The ASTM C1499 standard aims to ensure uniform stress within the load ring. However, for thin samples with relatively low elastic modulus (such as thin glass), the stress in the center is non-uniform[20]. This is because deformations are typically comparable to the sample thickness, so in-plane forces in the sample significantly change the stress distribution. For this reason, we built a finite element model using ADINA, which allows us to estimate the maximum stress in the glass as a function of the load force. The finite element model mesh (which uses shell elements with quadratic displacement interpolation functions) with a typical stress distribution is shown in Figure 14a. We treat this as a large deformation problem, which we found to have significantly different results than assuming small deformation. The mesh density was chosen based on convergence testing. The lower and left edges of the model are sliding-wall type boundary conditions, and the other edges are free. From this model, we determined the maximum stress in the glass as a function of the load. This is shown in Figure 14b.

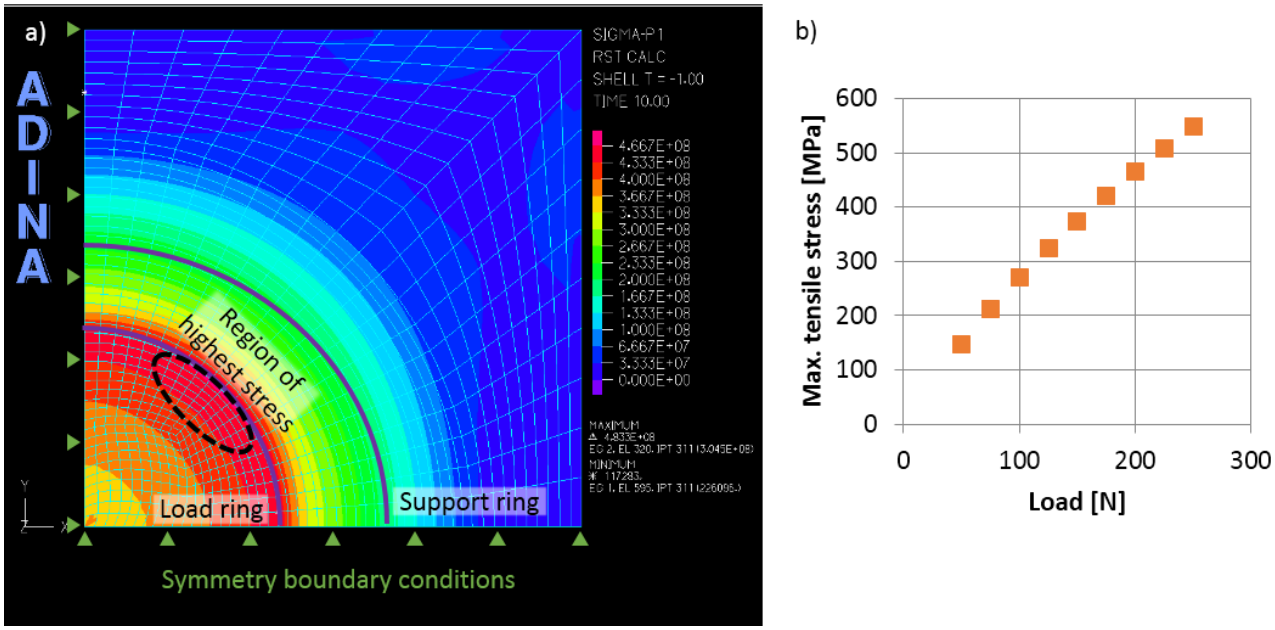

Figure 14. Finite element modeling results. a) Typical stress distribution (first principal stress) on the side of the glass under tensile stress. The symmetry boundary conditions are indicated. The element boundaries (9-node shell elements) are drawn in light blue. The region of highest stress is just inside of the load ring. The stress distribution is non-uniform in the center due to the large deformation of the glass. b) Calculated maximum first principal stress on the tensile-side surface. This relationship is non-linear due to the large deformation of the glass.

During the ion implantation, we only measure the curvature, and use a modified Stoney's equation to calculate the integrated stress. In order to estimate the local stress at the surface of the glass, we must make an assumption about the variation of stress as a function of depth in the glass. We do not have measurements for this distribution. We assume the stress varies linearly, with a maximum at the surface and vanishing to zero at the full depth of the implanted ions (4 μm). Under this assumption, the stress at the surface of the glass due to ion implantation, is

$$\sigma_{surface} = 2\frac{S}{d_{implant}},$$

where S is the integrated stress, $d_{implant}$ is the implant depth, and $\sigma_{surface}$ is the stress at the glass surface. The initial stress of the glass is assumed to be this implanted stress in the case of implanted samples, or zero in the other two groups of samples.

The strength results, shown in Figure 15, indicate that an initial tensile stress generally results in a decrease in strength, while an initial compressive stress generally results in an increase in strength. This is expected, since the glass fails due to tensile stresses propagating small surface defects. A linear regression shows that the breaking strength is reduced by approximately the same amount as the initial stress (the slope is approximately -1), although there are not enough data points to conclude this with certainty. The annealed samples show a reduced variance in strength compared to the as-supplied samples. This could possibly be explained if the annealing heals small surface defects, or reduces the size of defects. This could allow the glass to reach a higher load before a defect propogates to cause failure. There is also a noticeable strength offset of the implanted samples compared to the annealed samples. More data would be required to determine if this effect is real.

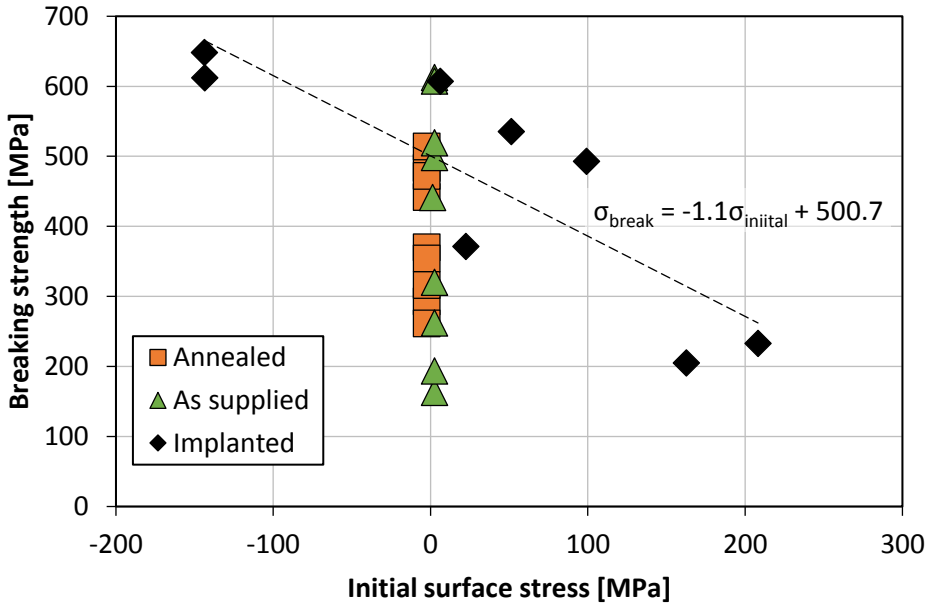

Figure 15. Strength testing results for Corning Eagle XG glass with various treatments. The Annealed and As supplied data points are slightly offset in the horizontal direction for clarity only (they are assumed to have zero initial stress). There is a clear trend in the implanted samples, indicated by the linear regression line, suggesting an initial tensile stress reduces the strength of the glass.

5. CONCLUSIONS

We have demonstrated stress-based figure correction using ion implantation in Schott D-263 glass wafers. We have found that significant post-implant changes in this material are significant, however. We have also measured stress resulting from ion implantation in fused silica, Corning Eagle XG glass, and crystalline silicon, and in these materials, post-implant changes are significantly smaller than for Schott D-263 glass. Finally, we have studied the effect of ion implantation on the strength of Eagle XG glass, and we have found that the implanted stress does affect the strength.

ACKNOWLEDGEMENTS

The authors would like to thank Will Zhang and the NGXO group at NASA Goddard Space Flight Center (GSFC), and Lester Cohen at Smithsonian Astrophysics Observatory (SAO) for helpful discussions. This work was financially supported by the NASA APRA grant NNX14AE76G, the MIT Kavli Institute Research Investment Fund, and the National Science Foundation Graduate Research Fellowship Program.

REFERENCES

[1] J. A. Gaskin, *et al.,* "The X-ray Surveyor Mission: A Concept Study," Proc. SPIE 96010J (2015).

[2] W. W. Zhang *et al.*, "Affordable and lightweight high-resolution x-ray optics for astronomical missions," Proc. SPIE 914415 (2014).

[3] R. Allured *et al.*, "Laboratory demonstration of the piezoelectric figure correction of a cylindrical slumped glass optic," Proc. SPIE 990554 (2016).

[4] M. L. Schattenburg, B. Chalifoux, M. D. DeTienne, R. K. Heilmann, and H. Zuo, "Progress report on air bearing slumping of thin glass mirrors for x-ray telescopes," Proc. SPIE 96030R (2015).

[5] W. W. Zhang *et al.*, "Lightweight and high-resolution single crystal silicon optics for x-ray astronomy," Proc. SPIE 99051S (2016).

[6] X. Wang, Y. Yao, T. Liu, C. Liu, M. P. Ulmer, and J. Cao, "Deformation of rectangular thin glass plate coated with magnetostrictive material," *Smart Mater. Struct.*, vol. 25, no. 8, p. 085038, 2016.

[7] K. Kilaru *et al.*, "Progress in differential deposition for improving the figures of full-shell astronomical grazing incidence x-ray optics," Proc. SPIE 96031F (2015).

[8] M. Ghigo *et al.*, "Ion figuring of large prototype mirror segments for the E-ELT," Proc. SPIE 91510Q (2014).

[9] B. Chalifoux, G. Wright, R. K. Heilmann, and M. L. Schattenburg, "Ion implantation for figure correction of thin X-ray telescope mirror substrates," Proc. SPIE 96031K (2015).

[10] B. Chalifoux, H. Zuo, G. Wright, Y. Yao, R. K. Heilmann, and M. L. Schattenburg, "Gas bearing slumping and figure correction of x-ray telescope mirror substrates," Proc. SPIE 990522 (2016).

[11] T. L. Aldcroft, D. A. Schwartz, P. B. Reid, V. Cotroneo, and W. N. Davis, "Simulating correction of adjustable optics for an x-ray telescope," Proc. SPIE 85030F (2012).

[12] C. R. Forest, *et al.*, "Metrology of thin transparent optics using Shack-Hartmann wavefront sensing," Opt. Eng. 43(3) 742-753 (2004).

[13] S. Suresh and L. B. Freund, *Thin Film Materials: Stress, Defect Formation and Surface Evolution*. Cambridge University Press, 2009.

[14] E. Snoeks, T. Weber, A. Cacciato, and A. Polman, "MeV ion irradiation-induced creation and relaxation of mechanical stress in silica," *J. Appl. Phys.*, vol. 78, no. 7, pp. 4723–4732, Oct. 1995.

[15] B. Chalifoux, E. Sung, R. K. Heilmann, and M. L. Schattenburg, "High-precision figure correction of x-ray telescope optics using ion implantation," Proc. SPIE 88610T (2013).

[16] C. A. Volkert, "Stress and plastic flow in silicon during amorphization by ion bombardment," J. Appl. Phys., 70, 3521 (1991).

[17] K.-W. Chan *et al.*, "Coating thin mirror segments for lightweight x-ray optics," Proc. SPIE 88610X (2013).

[18] D. M. Broadway *et al.*, "Achieving zero stress in iridium, chromium, and nickel thin films," Proc. SPIE 95100E (2015).

[19] K.-W. Chan *et al.*, "Reflective coating for lightweight x-ray optics," Proc. SPIE 84433S (2012).

[20] D. I. Wilcox, R. K. Akarapu, S. T. Gulati, S. Widjaja, and M. Antimonov, "Biaxial stress in thin glass during ring-on-ring testing with large deflections," *SID Symp. Dig. Tech. Pap.*, vol. 44, no. 1, pp. 874–876, Jun. 2013.